NASA/TP-2017-219590

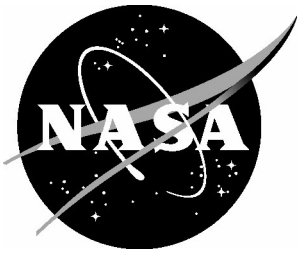

3DHZETRN: Inhomogeneous Geometry Issues

John W. Wilson
Old Dominion University, Norfolk, Virginia

Tony C. Slaba
Langley Research Center, Hampton, Virginia

Francis F. Badavi
Old Dominion University, Norfolk, Virginia

March 2017

NASA STI Program . . . in Profile

Since its founding, NASA has been dedicated to the advancement of aeronautics and space science. The NASA scientific and technical information (STI) program plays a key part in helping NASA maintain this important role.

The NASA STI program operates under the auspices of the Agency Chief Information Officer. It collects, organizes, provides for archiving, and disseminates NASA's STI. The NASA STI program provides access to the NTRS Registered and its public interface, the NASA Technical Reports Server, thus providing one of the largest collections of aeronautical and space science STI in the world. Results are published in both non-NASA channels and by NASA in the NASA STI Report Series, which includes the following report types:

- TECHNICAL PUBLICATION. Reports of completed research or a major significant phase of research that present the results of NASA Programs and include extensive data or theoretical analysis. Includes compilations of significant scientific and technical data and information deemed to be of continuing reference value. NASA counter-part of peer-reviewed formal professional papers but has less stringent limitations on manuscript length and extent of graphic presentations.

- TECHNICAL MEMORANDUM. Scientific and technical findings that are preliminary or of specialized interest, e.g., quick release reports, working papers, and bibliographies that contain minimal annotation. Does not contain extensive analysis.

- CONTRACTOR REPORT. Scientific and technical findings by NASA-sponsored contractors and grantees.

- CONFERENCE PUBLICATION. Collected papers from scientific and technical conferences, symposia, seminars, or other meetings sponsored or co-sponsored by NASA.

- SPECIAL PUBLICATION. Scientific, technical, or historical information from NASA programs, projects, and missions, often concerned with subjects having substantial public interest.

- TECHNICAL TRANSLATION. English-language translations of foreign scientific and technical material pertinent to NASA's mission.

Specialized services also include organizing and publishing research results, distributing specialized research announcements and feeds, providing information desk and personal search support, and enabling data exchange services.

For more information about the NASA STI program, see the following:

- Access the NASA STI program home page at http://www.sti.nasa.gov

- E-mail your question to help@sti.nasa.gov

- Phone the NASA STI Information Desk at 757-864-9658

- Write to:
  NASA STI Information Desk
  Mail Stop 148
  NASA Langley Research Center
  Hampton, VA 23681-2199

NASA/TP-2017-219590

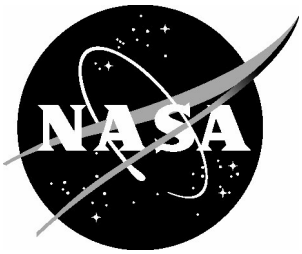

3DHZETRN: Inhomogeneous Geometry Issues

John W. Wilson
Old Dominion University, Norfolk, Virginia

Tony C. Slaba
Langley Research Center, Hampton, Virginia

Francis F. Badavi
Old Dominion University, Norfolk, Virginia

National Aeronautics and
Space Administration

Langley Research Center
Hampton, Virginia 23681-2199

March 2017

Available from:

NASA STI Program / Mail Stop 148
NASA Langley Research Center
Hampton, VA 23681-2199
Fax: 757-864-6500

Contents

Figures

Tables

Abstract

Historical methods for assessing radiation exposure inside complicated geometries for space applications were limited by computational constraints and lack of knowledge associated with nuclear processes occurring over a broad range of particles and energies. Various methods were developed and utilized to simplify geometric representations and enable coupling with simplified but efficient particle transport codes. Recent transport code development efforts, leading to 3DHZETRN, now enable such approximate methods to be carefully assessed to determine if past exposure analyses and validation efforts based on those approximate methods need to be revisited. In this work, historical methods of representing inhomogeneous spacecraft geometry for radiation protection analysis are first reviewed. Two inhomogeneous geometry cases, previously studied with 3DHZETRN and Monte Carlo codes, are considered with various levels of geometric approximation. Fluence, dose, and dose equivalent values are computed in all cases and compared. It is found that although these historical geometry approximations can induce large errors in neutron fluences up to 100 MeV, errors on dose and dose equivalent are modest (<10%) for the cases studied here.

Introduction

Traditionally, radiation protection meant isolating a sensitive material from the radiation source by shielding materials, distance, or time. For space operations with ubiquitous sources and mission dependent duration of exposure, radiation protection meant surrounding the sensitive materials to the extent possible with appropriate choice of shield materials. Many space system components are relatively open structures and offer little protection except over a restricted solid angle, leaving the pressure vessel and micrometeoroid bumper as the first line of inherent protection for space operations [Beever and Ruslino 1965, Slaba et al., 2011]. As a result of the high launch costs, minimizing the associated added weight of shield material is imperative to control mission costs [Shavers et al. 2003, Wilson et al. 2004], and consequently, there is a long history of developing engineering design strategies and methods for space operations [Krumbein et al. 1962, Robins 1965, Celnik et al. 1965, Atwell et al. 1979, 1987, Adamczyk et al. 2011, Walker et al. 2013, Simon et al. 2014].

Prior research identified radiations trapped within the Earth's magnetic field and solar particle events as the main concerns for protecting the astronauts and equipment from deleterious effects, so that protecting against moderate energy protons and energetic electrons became the focus of shield design and evaluation [Schaefer 1957, Foelsche 1962, Keller 1962]. As such, the atomic interactions were viewed as a primary driver of shielding design with optimization methods based on the scaling of atomic parameters [Krumbein et al. 1962], representing the range of penetration in units of mass per unit area (areal density). As attention turned to longer duration missions in deep space, it became apparent that the galactic cosmic rays might be the limiting factor [Foelsche 1959] (see Introduction of Wilson et al. [1991] for a review and Wilson et al. [1996] for a prospectus). In this case, the biological response to multiply charged ions of high energy and the means of reducing their effects with shielding was highly uncertain [Wilson et al. 1991]. Mitigation of radiation exposure from such ions remains a focus of current NASA radiation protection research (for background see Wilson et al. 1996).

The usual approach to shield design has been to first represent the spacecraft using combinatorial geometry (combinations of base objects as boxes, ellipsoids, cylinders etc.) and evaluate the average areal density (g/cm^2) of material in units of equivalent aluminum (eq. Al) within each given solid angle element of an equally divided unit sphere [Robins 1965, Liley and Schaedle 1965, Langley and Billings 1972, Atwell et al. 1987] and analyzing the transmission properties of each such sector. Various computer programs were developed to estimate the dose behind varying amounts of aluminum as given for each angular sector of the shield [Raymes 1965, Liley and Schaedle 1965, Simpson et al. 1965] and culminated in development of the HZETRN computer code [Wilson et al. 1991, 2005, 2006, Slaba et al. 2010, 2011]. Since the dose is reduced dramatically with increasing areal density of aluminum it was found that only the regions of minimal shielding contributed significantly to the dose [Keller 1962] and the most efficient shields are spherically symmetric [Wilson et al. 1993]. The first anthropomorphic model (Computerized Anatomical Man, CAM [Kase 1972]) was in units of equivalent aluminum to easily integrate into existing software [Atwell 1975]. Only later was the buildup factor method developed to more accurately represent dose and dose equivalent at a location in tissue behind an aluminum shield [Wilson and Kandelwal 1976, Wilson et al. 1991]. Additional work was done later to incorporate detailed voxel tissue phantoms [Slaba et al. 2009]. Since even isotropic sources of space radiation produce an anisotropic interior field within spacecraft, the orientation of the astronaut within a structure can produce differing organ exposures by a factor of two or more with changing

astronaut orientation [Wilson et al. 1993]. All of these past methods provided only one-dimensional (1D) approximations appropriate to each sector used in defining the geometric relations of the environment to dose or dose equivalent within an organ. Clearly, the angular dependence of secondary radiations produced in the shield will alter the solution within a given sector by diffusive losses from that sector that are not fully balanced by diffusion from adjacent sectors [Wilson et al. 2015a-c, Slaba et al. 2015].

Recently, an approach based on the straight-ahead/bi-directional approximations in HZETRN was extended into a three-dimensional (3D) code in which nuclear reactions within adjacent sectors are effective in modifying the fluence spectra along an adjacent ray [Wilson et al. 2015a,b]. Herein, this 3DHZETRN code will be used to evaluate the veracity of earlier work based on HZETRN (or other 1D codes) in which lateral diffusion is assumed balanced among adjacent sectors. In the present study, this 3DHZETRN code is used to examine the effects of differing geometric representations by evaluating the effects on dose, dose equivalent and spectral distributions within an International Commission on Radiation Units and Measurements (ICRU) tissue sphere [ICRU 1993] embedded within an aluminum structure.

3D Marching Procedures

The relevant transport description is the coupled linear Boltzmann equations derived on the basis of conservation principles [Wilson et al. 1991] for the flux (or fluence) density $\phi_j(\boldsymbol{x},\boldsymbol{\Omega},E)$ of a type j particle. In the continuous slowing down approximation [Wilson et al. 1991, 2005], in which atomic processes are described by the stopping power $S_j(E)$ for each ion type j (vanishes for neutrons, $j = n$), the transport equation is given as

$$\left[\boldsymbol{\Omega}\bullet\nabla - \frac{1}{A_j}\frac{\partial}{\partial E}S_j(E) + \sigma_j(E)\right]\phi_j(\boldsymbol{x},\boldsymbol{\Omega},E) = \sum_k \int_E^\infty \int_{4\pi} \sigma_{jk}(E,E',\boldsymbol{\Omega},\boldsymbol{\Omega}')\phi_k(\boldsymbol{x},\boldsymbol{\Omega}',E')\,d\boldsymbol{\Omega}'\,dE'\,, \tag{1}$$

and is solved subject to a boundary condition over the enclosure of the solution domain. In equation (1), $\sigma_j(E)$ and $\sigma_{jk}(E,E',\boldsymbol{\Omega},\boldsymbol{\Omega}')$ are the media macroscopic cross sections. The double differential cross section, $\sigma_{jk}(E,E',\boldsymbol{\Omega},\boldsymbol{\Omega}')$, represents all those processes by which type k particles moving in direction $\boldsymbol{\Omega}'$ with energy E' produce a type j particle in direction $\boldsymbol{\Omega}$ with energy E (including decay processes). A first approach to a computational procedure for solving equation (1) was to limit the interaction products to the forward direction (straight-ahead approximation) as

$$\sigma_{jk}(E,E',\boldsymbol{\Omega},\boldsymbol{\Omega}') = \sigma_{jk}(E,E')\delta(\boldsymbol{\Omega}-\boldsymbol{\Omega}')\,, \tag{2}$$

and is mainly an expression of approximate momentum conservation. Unlike the straight-ahead approximation that reduces equation (1) to a Volterra equation to be solved along a ray connected to the boundary, the first correction follows from a separation of the interaction into forward and isotropic components as

$$\sigma_{jk}(E,E',\boldsymbol{\Omega},\boldsymbol{\Omega}') = \frac{1}{4\pi}\sigma_{jk,iso}(E,E') + \sigma_{jk,for}(E,E',\boldsymbol{\Omega},\boldsymbol{\Omega}')\,, \tag{3}$$

wherein the fluence is separated as

$$\phi_j(\boldsymbol{x},\boldsymbol{\Omega},E) = \phi_{j,for}(\boldsymbol{x},\boldsymbol{\Omega},E) + \phi_{j,iso}(\boldsymbol{x},\boldsymbol{\Omega},E)\,. \tag{4}$$

The forward fluence, $\phi_{j,for}(\boldsymbol{x},\boldsymbol{\Omega},E)$, is defined to satisfy

$$\begin{aligned}\left[\boldsymbol{\Omega}\bullet\nabla - \frac{1}{A_j}\frac{\partial}{\partial E}S_j(E) + \sigma_j(E)\right]\phi_{j,for}(\boldsymbol{x},\boldsymbol{\Omega},E) \\ = \sum_k \int_E^\infty \int_{4\pi} \sigma_{jk,for}(E,E',\boldsymbol{\Omega},\boldsymbol{\Omega}')\phi_{k,for}(\boldsymbol{x},\boldsymbol{\Omega}',E')\,d\boldsymbol{\Omega}'\,dE'\end{aligned}\,, \tag{5}$$

and is solved using the straight-ahead approximation meeting the prescribed boundary conditions. The forward component generates an interior isotropic source of neutrons, $j = n$, given by

$$\xi_{n,iso}(\boldsymbol{x}, E, \boldsymbol{\Omega}, \boldsymbol{\Omega}_0) = \sum_k \int_E^\infty \int_{4\pi} \sigma_{nk,iso}(E, E', \boldsymbol{\Omega}, \boldsymbol{\Omega}_0) \phi_{k,for}(\boldsymbol{x}, \boldsymbol{\Omega}_0, E')\, dE' \quad , \tag{6}$$

that is the driving source generating the isotropic neutron perturbation field according to

$$\begin{aligned}[\boldsymbol{\Omega} \bullet \nabla + \sigma_n(E)]\phi_{n,iso}(\boldsymbol{x}, \boldsymbol{\Omega}, E) = &\sum_k \int_E^\infty \int_{4\pi} \sigma_{nk}(E, E', \boldsymbol{\Omega}, \boldsymbol{\Omega}')\phi_{k,iso}(\boldsymbol{x}, \boldsymbol{\Omega}', E')\, d\boldsymbol{\Omega}'\, dE' \\ &+ \xi_{n,iso}\left[z(\boldsymbol{x}), E, \boldsymbol{\Omega}, \boldsymbol{\Omega}_0\right]\end{aligned} \quad . \tag{7}$$

Whereas the forward field in equation (5) is solved for a given direction $\boldsymbol{\Omega}_0$ in the straight-ahead approximation, the field generated by the isotropic source in equation (7) is solved using the bi-directional approximation [Clowdsley et al. 2000, 2001] along an arbitrary ray $\boldsymbol{\Omega}$ (see Fig. 1). This solution of the Boltzmann equation is implemented in 3DHZETRN and has been shown to produce reasonable results for the isotropic neutron sources by comparison with various Monte Carlo simulations [Wilson et al. 2015a,b].

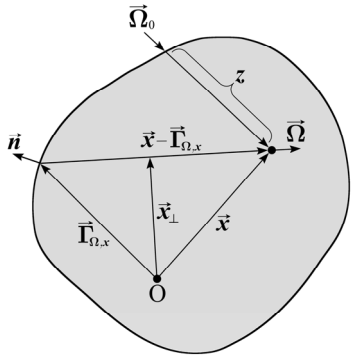

Fig. 1. Geometric relations of quantities useful in solving equation (1). The symbol $\vec{n}$ is a unit normal vector.

Geometry/Material Selection

Since space radiation protection is the design of the material arrangement about a sensitive volume, how the geometry and materials are chosen to provide adequate protection is at issue [Wilson et al. 2004]. Many materials are chosen according to other functional requirements/properties. For example, structural aluminum has been chosen in the past for construction of spacecraft pressure vessels, micrometeoroid bumper, and support structures. More recent technologies are switching to polymer-composites to capitalize on their strength to weight ratios and improved radiation protection properties. Foodstuffs and water have always been part of the inherent shielding [Wilson 2000] and encapsulated polyethylene has been used for shield augmentation because of its improved shielding quality and low launch costs [Shavers et al. 2003].

Spherical Geometries

In this section, the geometry of interest is an aluminum spherical shell with a thickness of 7.41 cm (20 g/cm^2) surrounding an inner 30 cm diameter (30 g/cm^2) ICRU [1993] tissue sphere (astronaut proxy) separated by a 1 m void as shown in Fig. 2. The external radiation environment, taken here as the Webber [1966] representation of the 1956 solar particle event, is assumed to be anti-parallel with the z-axis, uniform in the x-y plane, positioned above the geometry and directed down along $\boldsymbol{\Omega}_0$. The fluence, dose, and dose equivalent will be computed using 3DHZETRN at the top and bottom of the tissue sphere; these values will be used as a baseline for comparison against related geometric representations derived with approximations used in the past.

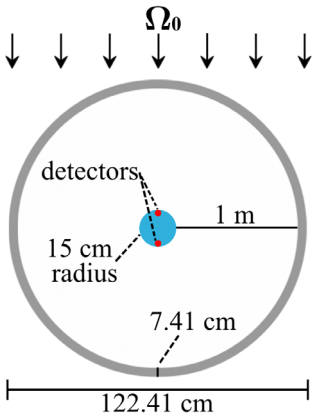

Fig. 2. A 30 cm diameter ICRU sphere within a 7.41 cm thick aluminum shell with a 1 m void (referred to as "orig. geom." in subsequent figures and tables).

The first geometric simplification to be considered represents the materials in linear dimensions (cm) as they occur within the geometry, but the void region is eliminated, as shown in Fig. 3. Fluences obtained in the spherical geometry with and without the voids are shown in Fig. 4. It is clear that removal of the void results in a perturbation of mainly the neutron field up to ~200 MeV but also in the charged particle fields below ~10 MeV.

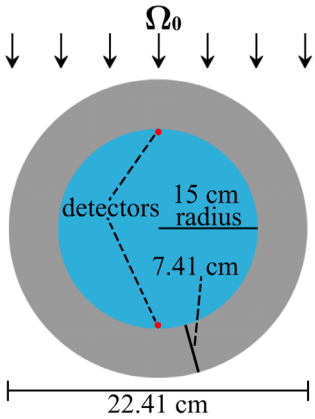

Fig. 3. A 30 cm diameter ICRU sphere within a 7.41 cm thick aluminum shell (referred to as "void removed" in subsequent figures and tables).

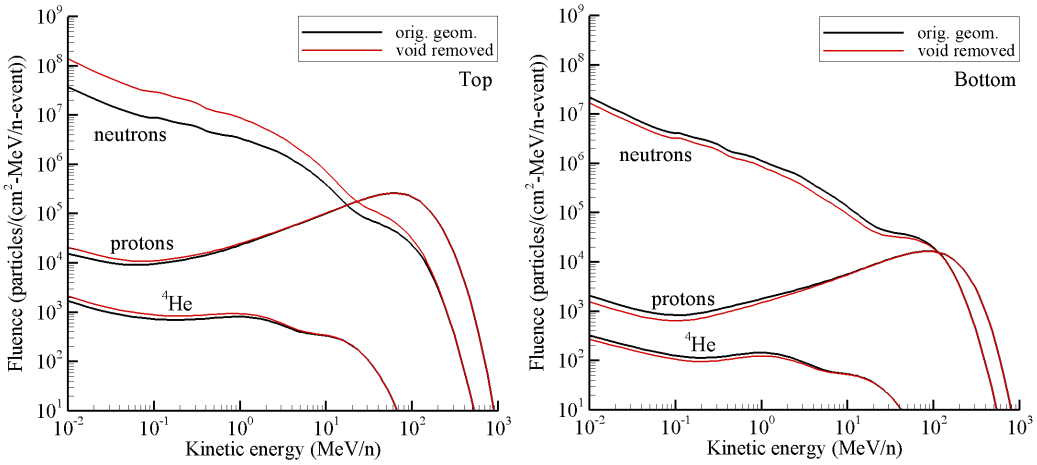

Fig. 4. The effects on the particle fields at the top and bottom of the sphere induced by removing the void in Fig. 2.

In sector analysis, it is customary to use dimensions of g/cm^2, thereby eliminating all void regions with nearly 0 g/cm^2 of material [Robins 1965, Raymes 1965] and introducing further geometric distortion, as shown in Fig. 5.

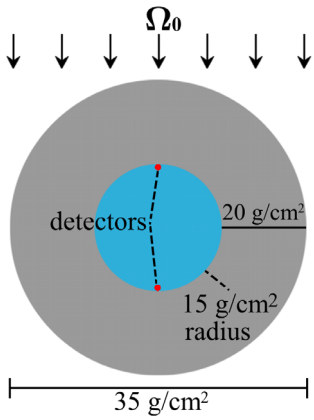

Fig 5. A 30 g/cm^2 diameter ICRU sphere within a 20 g/cm^2 thick aluminum shell in g/cm^2 scale (referred to as "g/cm^2 geom." in subsequent figures and tables).

Even more extreme assumptions have been used in the past by replacing various materials with an equivalent amount of aluminum by scaling according to the primary incident protons and their atomic interactions in the specific materials as discussed above [Walker et al. 2011]. In the example considered presently, the tissue sphere is replaced by an equivalent aluminum sphere, where the aluminum sphere radius is computed as

$$x_{eq,Al} = \frac{R_{p,Al}(50)}{R_{p,tissue}(50)} x_{tissue} \ . \tag{8}$$

In equation (8), x_{tissue} = 15 g/cm^2 is the original tissue thickness, $R_{p,Al}(50)$ = 2.92 g/cm^2 is the range of a 50 MeV proton in aluminum, $R_{p,tissue}(50)$ = 2.22 g/cm^2 is the range of a 50 MeV proton in tissue, and $x_{eq,Al}$ = 19.73 g/cm^2 is the equivalent aluminum thickness. The equivalent aluminum approximate geometry is shown in Fig. 6.

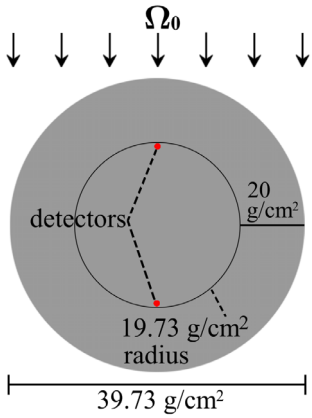

Fig. 6. A 30 g/cm^2 diameter ICRU sphere made of equivalent aluminum within a 20 g/cm^2 thick aluminum shell (referred to as "eq. Al geom." in subsequent figures and tables).

The three approximate geometries of Figs. 3, 5, and 6 are analyzed using the 3DHZETRN code and compared with results derived from the original geometry (Fig. 2) with resultant fluence shown in Fig. 7. To better emphasize the differences in neutron fluence, the results are given as ratios in Fig. 8, where the results for the approximate geometries are divided by the result for the original geometry. As expected, a large error occurs in replacing the tissue by equivalent aluminum. This approximation is based on the assumption that atomic processes reasonably scale from one material to another and ignores the fact that nuclear interactions (cross sections) are strongly material dependent and do not scale in this way. Atomic interactions are largely dependent on the electron density within the material with only somewhat small binding corrections [Krumbein et al. 1962]. As a result, the atomic processes depend only on the nuclear charge in distinction to nuclear processes that depend on not only the nuclear charge but strongly dependent on the nuclear mass.

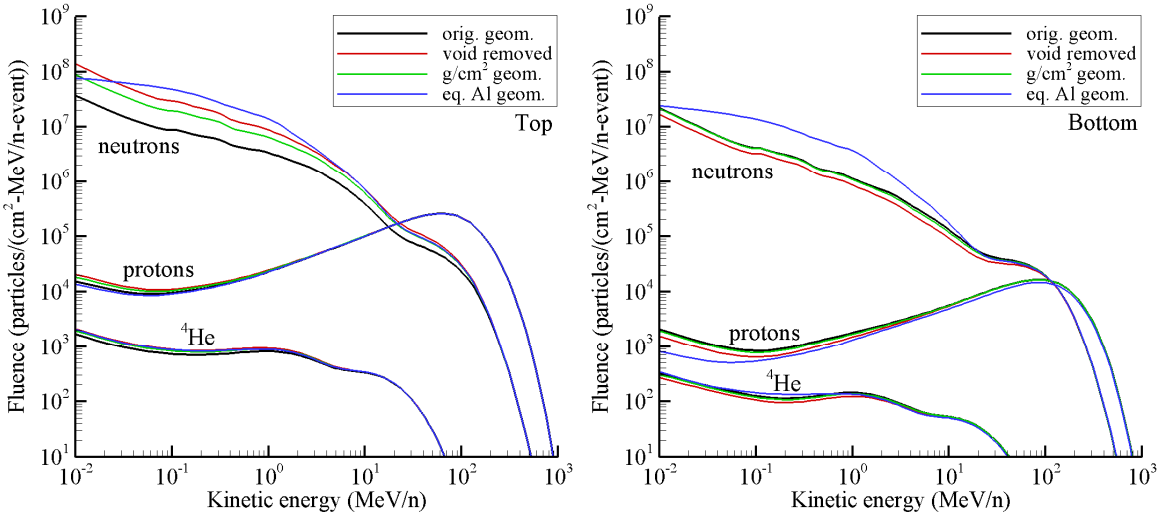

Fig. 7. 3DHZETRN results of fluence vs. kinetic energy for detectors at the top and bottom of an ICRU tissue sphere within an aluminum shell for the configuration depicted in Figs. 2, 3, 5, and 6.

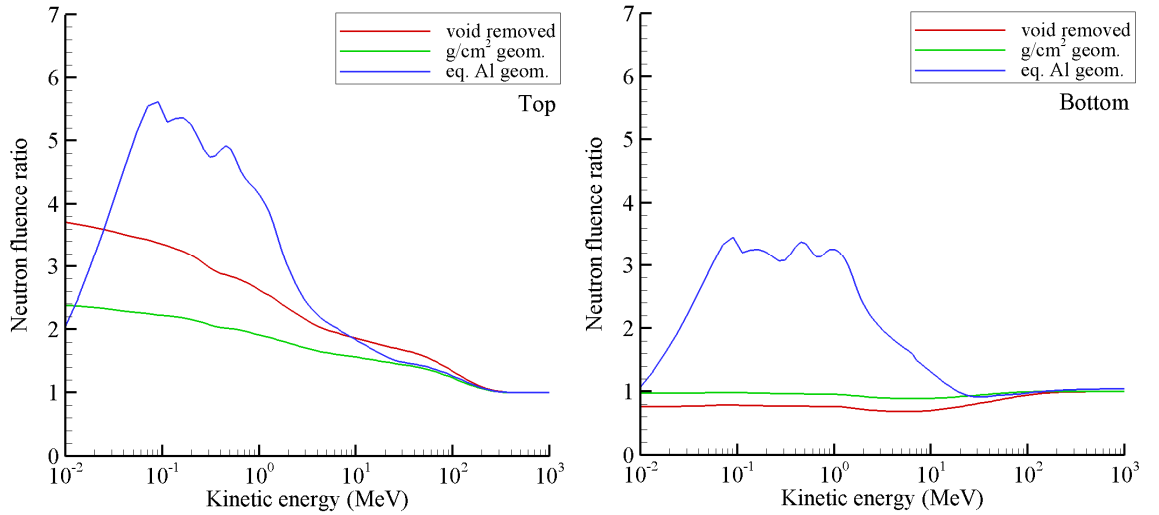

Fig. 8. Neutron fluence ratios for the approximate geometries (Figs. 3, 5, and 6) relative to solutions of the original geometry (Fig. 2).

Figs. 7 and 8 show that the various geometric approximations can induce large differences in the neutron fluence. However, the impact on dose and dose equivalent values, as seen in Table 1, is not as severe. Table 2 gives the relative differences between the original and approximate geometry results previously given in Table 1. The relative differences are on the order of ten percent or less and may be significant depending on the approximation used. Clearly, use of the native geometry is the reliable method for evaluation.

Table 1. Dose and dose equivalent at top and bottom of tissue sphere contained within an aluminum shell represented with various levels of approximation.

Geometry	Dose (cGy)		Dose equivalent (cSv)	
	Top	Bottom	Top	Bottom
orig. geom.	6.99	0.51	10.87	1.06
void removed	7.06	0.50	11.92	0.95
g/cm^2 geom.	7.04	0.51	11.50	1.03
eq. Al geom.	7.04	0.46	11.86	1.14

Table 2. Relative differences (%) between values in Table 1 for geometry with void region compared to values for various levels of approximation.

Geometry	Dose (%)		Dose equivalent (%)	
	Top	Bottom	Top	Bottom
void removed	0.93	-1.81	9.50	-8.52
g/cm^2 geom.	0.55	-0.68	5.34	-3.10
eq. Al geom.	0.70	-9.97	9.19	8.33

Complex Geometries

In this example, a more complex geometry is considered. It consists of a 30 cm diameter tissue equivalent sphere [ICRU 1993] shielded by a 2.47 cm (5 g/cm^2) thick truncated cylindrical aluminum shell (diameter 75 cm, length 175 cm) with 4.94 cm (10 g/cm^2) thick end caps as shown in Fig. 9. In addition to the ICRU sphere at the center of the aluminum cylindrical shell, an interior aluminum box with dimensions 125×40×40 g/cm^2 (yellow box in upper portion of Fig. 9) and a second aluminum box with dimensions 60×60×100 g/cm^2 (red box in lower portion of Fig. 9) are also included. As in the previous section, the external radiation environment is taken here as the Webber [1966] representation of the 1956 solar particle event and assumed to be oriented anti-parallel with the *z*-axis, uniform in the *x*-*y* plane, positioned above the geometry and directed down along $\mathbf{\Omega}_0$. The fluence, dose, and dose equivalent are computed at the top and bottom detector locations using 3DHZETRN as in the previous section. This geometry and boundary condition configuration has been extensively studied using Monte Carlo (MC) simulation to allow testing of the 3DHZETRN computational procedures in a realistic combinatorial geometry.

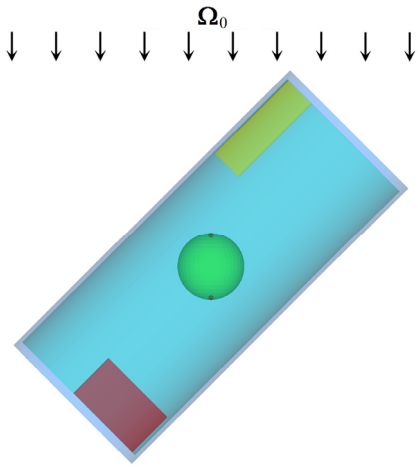

Fig. 9. Complex geometry used in the current study: ICRU tissue sphere shielded by an aluminum cylindrical shell with internal components (referred to as "orig. geom." in subsequent figures and tables).

The resultant fluences are given in Fig. 10 for the shield arrangement with the voids included as shown in Fig. 9, after removing the voids (collapsed), expressing the collapsed geometry in g/cm^2, and replacing the tissue sphere by an equivalent aluminum sphere. Only minor differences are seen in the light ion fluences at the lowest energies, but large differences in the neutron fluence are observed up to 100 MeV, especially when the tissue sphere is replaced by an equivalent aluminum sphere. The ratio of the neutron fluence results computed in the approximate geometry to the results computed in the original geometry arrangement is shown in Fig. 11. The neutron fluence below 100 MeV is overestimated by a factor of 2 as a result of simply removing the void, but does not appear to depend heavily on switching between cm and g/cm^2 length scales. There is little variation in fluence at the bottom of the sphere for the approximate geometries in terms of cm and g/cm^2 relative to the original geometry. In an isotropic environment (as expected in a real solar particle event) the results at top and bottom become averaged. It is seen that even under isotropic conditions, the traditional equivalent aluminum approximation is not a good substitute for the actual geometry.

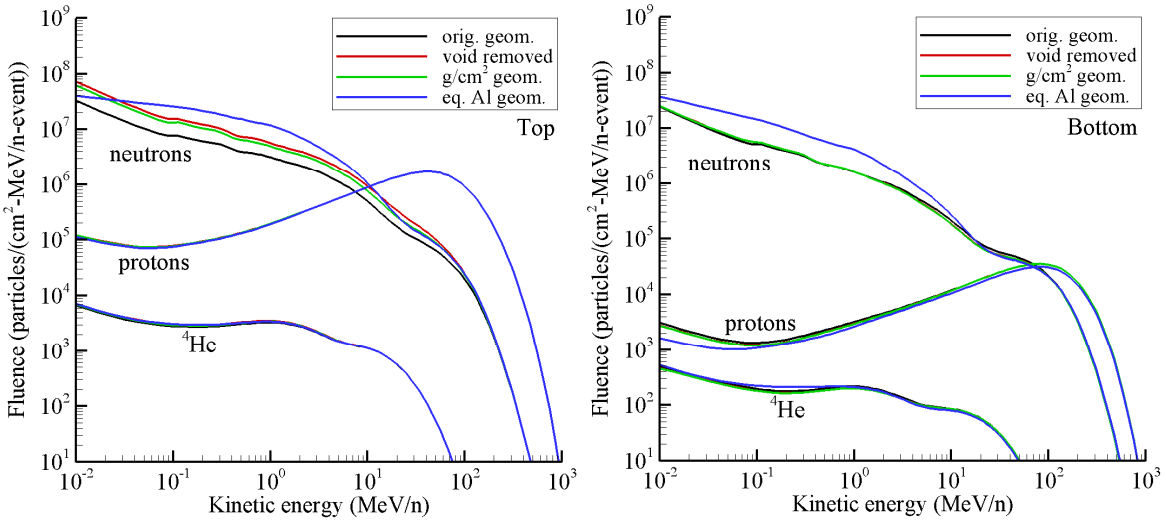

Fig. 10. Fluence spectra in complex geometry for detectors at the top and bottom of the geometry configuration depicted in Fig. 9 and related approximate geometries.

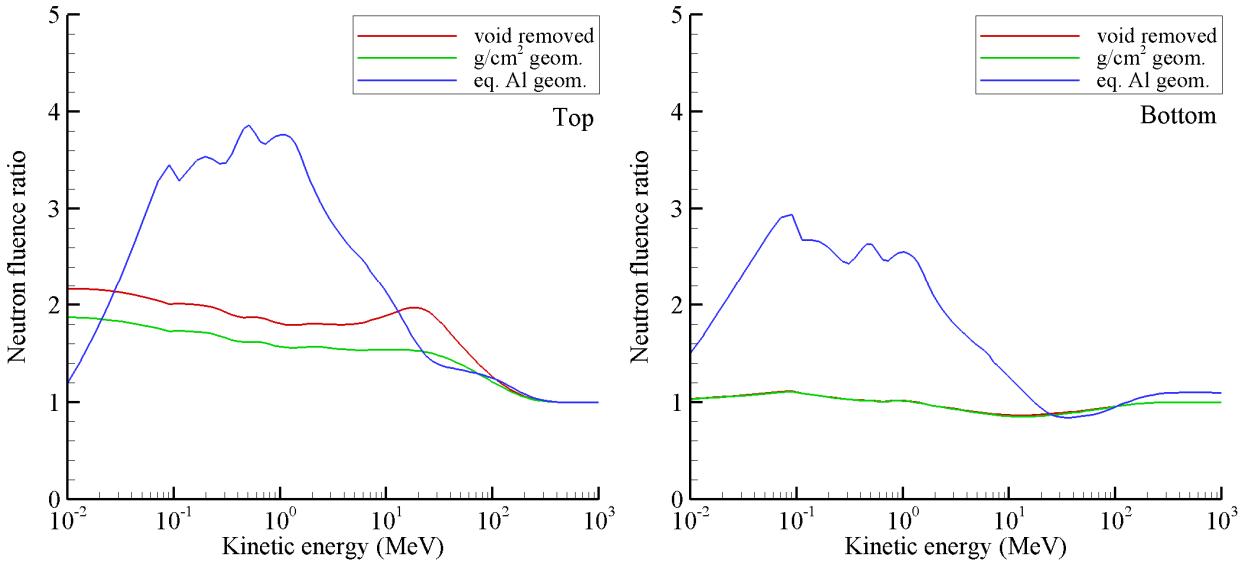

Fig. 11. Neutron fluence ratios in complex geometry for the approximate geometries relative to solutions of the original geometry.

Although there are large differences in the neutron fluence for all three approximate geometries compared to the original geometry, the impact on dose and dose equivalent values, as seen in Table 3, is modest. Relative differences between values in Table 3 for the original geometry with void region compared to values for various approximate geometries are provided in Table 4. Only the results computed in equivalent aluminum approximate geometry exhibit significant differences (see Table 4 at bottom detector) for this mono-directional case. For isotropic incidence, the errors in the three approximate geometries are expected to behave like the average of the top and the bottom.

In the past, various approximations were used to make the problem of estimating dosimetric quantities practical within the limitations of knowledge of physical parameters and computational procedures. With improvements in knowledge, procedures, and computational speed over the last four decades, there is no need to make such approximations. Results presented herein suggest there is no need to correct past results from a geometric point of view, although issues related to knowledge of the response of instruments and conversion to dosimetric quantities remain. With modern computational procedures, the main development remains to improve knowledge of physical interaction parameters, continued improvement of computational procedures and improved understanding of the driving physical parameters as related to biological response [Wilson 2000].

Table 3. Dose and dose equivalent in complex geometry at top and bottom of tissue sphere contained within an aluminum shell represented with various levels of approximation.

Geometry	Dose (cGy)		Dose equivalent (cSv)	
	Top	Bottom	Top	Bottom
orig. geom.	42.78	1.04	65.89	1.90
void removed	42.88	1.04	66.94	1.84
g/cm^2 geom.	42.85	1.04	66.57	1.84
eq. Al geom.	42.81	0.94	66.77	1.94

Table 4. Relative differences (%) between values in Table 3 for geometry with void region compared to values for various approximate geometries.

Geometry	Dose (%)		Dose equivalent (%)	
	Top	Bottom	Top	Bottom
void removed	0.23	-0.64	1.60	-3.08
g/cm^2 geom.	0.15	-0.69	1.04	-3.33
eq. Al geom.	0.07	-10.34	1.33	2.06

Conclusions

Methods examined in this work and used in the past for radiation analysis of spacecraft included sector analysis in which voids between components are eliminated within the sector, or replaced by areal density (g/cm^2), or in other instances replaced all areal density of each material by equivalent areal density of aluminum. Each approximation results in distortions in the geometry and was shown to affect computational results where 3D effects are of importance (especially for neutrons with large diffusion coefficients). Even the most benign approximation of removing voids has a significant effect on the neutron fluence below 100 MeV of up to a factor of four depending on the geometry. Even so, the effect on dose and dose equivalent is a more modest error of up to 10 percent depending on geometric detail. The effect of further changing from linear scale (cm) to areal density (g/cm^2) scale are similarly distorted transport results. Still more inaccurate is the replacement of materials by equivalent aluminum (areal density), which includes not just geometric distortions but also affects atomic and especially nuclear properties.

Acknowledgements

This work was supported by the Human Research Program under the Human Exploration and Operations Mission Directorate of NASA and by NASA Grant number NNX09AR20A.

References

Adamczyk, A., Clowdsley, M.S., Qualls, G.D., Blattnig, S.R., Lee, K.T., Fry, D., Stoffle, N., Simonsen, L.C., Slaba, T.C., Walker, S.A., Zapp, E., "Full Mission Astronaut Radiation Exposure Assessment for Long Duration Lunar Surface Missions", Proceedings of IEEE Aerospace Conference, March 5-12, 2011.

Atwell, W., "Man Model Mass Distributions Using the Least Squares and Regula Falsi Methods", Rockwell-Houston Internal Memo; 1975.

Atwell, W., Beever, E.R., "SHLDAT-Analytical Shielding Model of the Space Shuttle", Rockwell-Houston Internal Memo; 1979.

Atwell, W., Beever, E.R., Hardy, A.C., "Radiation Shielding Analysis for the Space Shuttle Program: An Overview", American Nuclear Society, Topical Conference on Theory and Practices in Radiation Protection and Shielding, Knoxville, TN, (published in ISBN: 0-89448-132-0, PP. 271-280); 1987.

Beever, E.R., Ruslino, D.H., "The Importance of Space Radiation Shielding Weight", Second Symposium on Protection against Radiation in Space, NASA SP-71, 407-414; 1965.

Clowdsley, M.S., Heinbockel, J.H., Kaneko, H., Wilson, J.W., Singleterry, R.C., Shinn, J.L., "A Comparison of the Multi-group and Collocation Methods for Solving the Low-energy Neutron Boltzmann Equation", Can. J. Phys., vol. 78, 45-56; 2000.

Clowdsley, M.S., Wilson, J.W., Shinn, J.L., Badavi, F.F., Heinbockel, J.H., Atwell, W., "Neutron Environment Calculations for Low Earth Orbit", SAE-ICES-2327; 2001.

Celnik, J., Krumbien, A.D., Nakache, F.R., "Synthesis of Spherical Minimum-Weight Proton Shields", Second Symposium on Protection Against Radiation in Space, NASA SP-71, 225-229; 1965.

Foelsche, T., "Estimate of the Specific Ionization Caused by Heavy Cosmic Ray Primaries in Tissue or Water", J. Astronaut. Sci. vol. VI (4), 57-62; 1959.

Foelsche, T., "Protection Against Solar Flare Protons", Advances in the Astronautical Sciences, vol. 8, Plenum Press Inc, 357-374; 1962.

ICRU International Commission on Radiation Units and Measurements, Quantities and Units in Radiation Protection Dosimetry, ICRU Report 51; 1993.

Kase, P.G., "Influence of a Detailed Model of Man on Proton Depth/Dose Calculations", Proceedings of the National Symposium on Natural and Manmade Radiation in Space, NASA TM X-2440, 773-780; 1972.

Keller, J.W., "Long Range NASA Shielding Requirements", Proceedings of the Symposium on the Protection against Radiation Hazards in Space, TID-7652, 662-681; 1962.

Krumbein, A.D., Mittelman, P.S., Troubetzkoy, E.S., Nakache, F., Celnik, J., "Synthesis of Minimum Weight Proton Shields", Proceedings of the Symposium on the Protection Against Radiation Hazards in Space, AEC TID-7652; 1962.

Langley, R.W., Billings, M.P., "Methods of Space Radiation Dose Analysis with Applications to Manned Space Systems", Proceedings of the National Symposium on Natural and Manmade Radiation in Space", NASA TM X-2440, 108-116; 1972.

Liley, B., Schaedle, G.C., "An Examination of the Relative Merits of Stochastic and Non-statistical Methods of Computing Primary Ionization Doses", Second Symposium on Protection Against Radiation in Space, NASA SP-71, 527-534; 1965.

Raymes, F.I., "Apollo Spacecraft Nuclear Radiation Status Report", Second Symposium on Protection against Radiation in Space, NASA SP-71, 365-375; 1965.

Robins, D.F., "Status Report on the Space Radiation Effects on the Apollo Mission: B. Apollo Shielding Analysis", Second Symposium on Protection Against Radiation in Space, NASA SP-71, 143-147; 1965.

Schaefer, H.J., "Cosmic Ray Dosage During the Giant Solar Flare of February 23, 1956", J. Aviation Med., vol. 28, 387-396; 1957.

Shavers, M.R., Zapp, N., Barber, R.E., Wilson, J.W., Qualls, G., Toupes, L., Ramsey, S., Vinci, V., Smith, G., Cucinotta, F.A., "Implementation of ALARA Radiation Protection on the ISS through Polyethylene Shielding Augmentation of the Service Module Crew Quarters", Adv. Space Res., vol. 34(6),1333-1337; 2003.

Simon, M.A., Cerro J.A., Latorella, K., Clowdsley, M.S., Watson, J., Albertson, C., Norman, R., Le Boffe, V., Walker, S., "Design of Two RadWorks Storm Shelters for Solar Particle Event Shielding", AIAA Info. Space 2014.

Simpson, K.M., Hill, C.W., Douglass, C.C., "Space Radiation Shielding Code For Realistic Vehicle Geometries", Second Symposium on Protection Against Radiation in Space, NASA SP-71, 534-539; 1965.

Slaba, T.C., Qualls, G.D., Clowdsley, M.S., Blattnig S.R., Simonsen, L.C., Walker, S.A., Singleterry, R.C., Analysis of Mass Averaged Tissue Doses in CAM, CAF, MAX, and FAX", NASA TP 215562, 2009.

Slaba, T.C., Blattnig, S.R., Badavi, F.F., "Faster and more Accurate Transport Procedures for HZETRN", J. Comp. Phys. vol. 229, 9397-9417; 2010.

Slaba, T.C., Blattnig, S.R., Clowdsley, M.S., "Variation in Lunar Neutron Dose Estimates", Rad. Res., vol. 176, 827-841, 2011.

Slaba, T.C, .Wilson, J.W., Badavi, F.F., Reddell, B.D., Bahadori, A.A., "Solar Proton Transport within an ICRU Sphere Surrounded by a Complex Shield: Ray-trace Geometry", NASA TP-218994; 2015.

Walker, S.A., Slaba, T.C., Clowdsley, M.S., Blattnig, S.R., "Investigating Material Approximations in Spacecraft Radiation Analysis", Acta. Astro. vol. 69, 6-17, 2011.

Walker S.A., Clowdsley M.S., Abston H.L., Simon, M.A., Gallegos A.M., "Radiation Exposure Analyses Supporting the Development of Solar Particle Event Shielding Technologies", 43rd ICES, AIAA 2013-3042, July 14-18, 2013.

Webber, W.R., "An Evaluation of Solar-Cosmic-Ray Events during Solar Minimum", D2-84274-1, Boeing Co.; 1966.

Wilson, J.W. Khandelwal, G.S., "Proton-Tissue Dose Buildup Factors", Health Phys., vol. 31(2), 115-118; 1976.

Wilson, J.W., Townsend, L.W., Schimmerling, W., Khandelwal, G.S., Khan, F., Nealy, J.E., Cucinotta, F.A., Simonsen, L. ., Shinn, J L., Norbury, J. W., "Transport Methods and Interactions for Space Radiations. NASA RP-1257; 1991.

Wilson, J.W., Nealy, J.E., Wood, J.S., Qualls, G., Atwell, W., Shinn, J.L., Simonsen, L.C., "Exposure Fluctuations of Astronauts due to Orientation", NASA TP 3364; 1993.

Wilson, J.W., Cucinotta, F.A., Miller, J., "Radiation Shielding Issues in Highly Inclined Low Earth Orbits", SAE Technical Paper 961581; 1996.

Wilson, J.W., "Overview of Radiation Environments and Human Exposures", Health Phys., vol. 79, 470-94; 2000.

Wilson, J.W., Cucinotta, F.A., Schimmerling, W.S., "Emerging Radiation Health-Risk Mitigation Technologies", AIP Conf. Proc. 699, 913-924; 2004.

Wilson, J.W., Tripathi, R.K., Mertens, C.J., Blattnig, S.R., Clowdsley, M.S., "Verification and Validation: High Charge and Energy (HZE) Transport Codes and Future Development", NASA TP-213784; 2005.

Wilson, J.W., Tripathi, R.K., Badavi, F.F., Cucinotta, F.A., "Standardized Radiation Shield Design Method: 2005 HZETRN", SAE/ICES paper 01-2109; 2006.

Wilson, J.W., Slaba, T.C., Badavi, F.F., Reddell, B.D., Bahadori, A.A., "3DHZETRN: Shielded ICRU Spherical Phantom", Life Sci. Space Res., vol. 4, 46-61; 2015a.

Wilson, J.W., Slaba, T.C., Badavi, F.F., Reddell, B.D., Bahadori, A.A., "Solar Proton Transport within an ICRU Sphere Surrounded by a Complex Shield: Combinatorial Geometry", NASA TP-218980; 2015b.

Wilson, J.W., Slaba, T.C., Badavi, F.F., Reddell, B.D., Bahadori, A.A., "A Study of Neutron Leakage in Finite Objects", Life Sci. Space Res., vol. 7, 27–38; 2015c.

REPORT DOCUMENTATION PAGE

Form Approved
OMB No. 0704-0188

1. REPORT DATE *(DD-MM-YYYY)*	2. REPORT TYPE	3. DATES COVERED *(From - To)*
01- 03 - 2017	Technical Publication	

4. TITLE AND SUBTITLE

3DHZETRN: Inhomogeneous Geometry Issues

5a. CONTRACT NUMBER

5b. GRANT NUMBER

5c. PROGRAM ELEMENT NUMBER

6. AUTHOR(S)

Wilson, John W.; Slaba, Tony C.; Badavi, Francis F.

5d. PROJECT NUMBER

5e. TASK NUMBER

5f. WORK UNIT NUMBER

651549.02.07.10

7. PERFORMING ORGANIZATION NAME(S) AND ADDRESS(ES)

NASA Langley Research Center
Hampton, VA 23681-2199

8. PERFORMING ORGANIZATION REPORT NUMBER

L-20786

9. SPONSORING/MONITORING AGENCY NAME(S) AND ADDRESS(ES)

National Aeronautics and Space Administration
Washington, DC 20546-0001

10. SPONSOR/MONITOR'S ACRONYM(S)

NASA

11. SPONSOR/MONITOR'S REPORT NUMBER(S)

NASA-TM-2017-219590

12. DISTRIBUTION/AVAILABILITY STATEMENT

Unclassified - Unlimited
Subject Category 93
Availability: NASA STI Program (757) 864-9658

13. SUPPLEMENTARY NOTES

14. ABSTRACT

Historical methods for assessing radiation exposure inside complicated geometries for space applications were limited by computational constraints and lack of knowledge associated with nuclear processes occurring over a broad range of particles and energies. Various methods were developed and utilized to simplify geometric representations and enable coupling with simplified but efficient particle transport codes. Recent transport code development efforts, leading to 3DHZETRN, now enable such approximate methods to be carefully assessed to determine if past exposure analyses and validation efforts based on those approximate methods need to be revisited. In this work, historical methods of representing inhomogeneous spacecraft geometry for radiation protection analysis are first reviewed. Two inhomogeneous geometry cases, previously studied with 3DHZETRN and Monte Carlo codes, are considered with various levels of geometric approximation. Fluence, dose, and dose equivalent values are computed in all cases and compared. It is found that although these historical geometry approximations can induce large errors in neutron fluences up to 100 MeV, errors on dose and dose equivalent are modest (<10%) for the cases studied here.

15. SUBJECT TERMS

HZETRN; Radiation

16. SECURITY CLASSIFICATION OF:			17. LIMITATION OF ABSTRACT	18. NUMBER OF PAGES	19a. NAME OF RESPONSIBLE PERSON
a. REPORT	b. ABSTRACT	c. THIS PAGE			STI Help Desk (email: help@sti.nasa.gov)
U	U	U	UU	20	19b. TELEPHONE NUMBER *(Include area code)* (757) 864-9658